Asian Journal of Chemistry; Vol. 35, No. 6 (2023), 1361-1368

ASIAN JOURNAL OF CHEMISTRY

https://doi.org/10.14233/ajchem.2023.27741

Development of Nano-Hydroxyapatite Polymer Composite and it's *in vitro* Activity for Biomedical Applications

S. MARY STELLA and U. VIJAYALAKSHMI*

Department of Chemistry, School of Advanced Sciences, Vellore Institute of Technology, Vellore-632014, India

*Corresponding author: Fax: +91 416 224 3092; Tel: +91 416 2202464; E-mail: lakesminat@yahoo.com

Received: 9 March 2023; *Accepted*: 13 April 2023; *Published online*: 27 May 2023; AJC-21251

In present work, the composites of hydroxyapatite with polyvinyl alcohol (PVA) and polyvinyl pyrrolidone (PVP) were prepared and analyzed for its biodegradability and hemocompatibilty. The individual and the combined combination of polymers with hydroxyapatite (HAP-PVA, HAP-PVP and HAP/PVA-PVP) were characterized by FT-IR, XRD, SEM-EDAX and TGA-DSC analysis. The crystallinity and functional groups of hydroxyapatite (HAP) was confirmed by XRD and FT-IR analysis. The SEM analysis displayed rod shaped morphology and the formation of apatite layer was confirmed by simulated body fluid (SBF) immersion. The Ca/P ratio of the SBF immersed composite was found to be increased to 1.71. This reveals that the polymer in the composite acts as a nucleating site for the development of carbonated hydroxyapatite which chemical composition resembles with natural bone. The hemolysis rate for the composite consisting of HAP/PVA-PVP was found to be less than 3% than the composite consisting of HAP with PVP. Based on these results, it can be concluded that the HAP/PVA-PVP nanocomposite offers superior alternatives in the field of biomedicines.

Keywords: Biocompatibility, Hemocompatibility, Hydroxyapatite, Nanocomposite, Polymers.

INTRODUCTION

In recent approaches, the replacement of damaged bone in the major approaches is through orthopedic surgeries. Synthetic scaffolds in bone tissue engineering own several significant characteristics such as biocompatibility, mechanical strength, biodegradation, osteoconductivity and osteoinductivity for bone regeneration process. Composite made of ceramics and polymers plays a significant key role in bone grafting [1,2]. Bioactive ceramics such as hydroxyapatite (HAP), tricalcium phosphate (TCP), silicate glasses (bioactive glasses) and glass-ceramics respond towards physiological fluids by the formation of hard and soft tissues on the implant. Compared with other ceramics, hydroxyapatite (HAP, $Ca_{10}(PO_4)_6(OH)_2$) resembles the natural bone composition in context to chemical composition and also attains biocompatible or bioactivity nature [3,4]. It exhibits more biocompatibility by forming a strong bond with natural bone. Besides its good characteristics, it has low degradability and brittleness, which limits its application to biomedical field. However, the mechanical property can be enhanced by combining with polymer, which promotes bone regeneration.

Many researchers have focused on various types of polymers such as natural polymers (chitosan, silk, gelatin, elastin, keratin, fibrin, collagen, hyaluronic acid and starch) and synthetic polymers (poly lactic acid (PLA), poly glycolic acid (PGA), poly-(L-lactic acid) (PLLA), poly(L-lactic-*co*-glycolic acid) (PLGA), polyvinyl alcohol (PVA), polyvinyl pyrrolidone (PVP), poly-(hydroxybutyrate-*co*-hydroxyvalerate) (PHBV), polyurethane, polycaprolactone (PCL)) [5,6]. These polymers encapsulates the cells easily hence improving the cell adhesion, proliferation and differentiation. Compared to natural polymer, the synthetic polymers have improved mechanical property (tensile strength, elastic modulus) and are majorly used in biomedical applications [7]. As PVA and PVP polymers are commercially available, low-cost, bio-inert and less toxic and hence used as an additive in major biomedical applications [8,9].

Composites made of hydroxyapatite with various polymer combinations have shown good biocompatibility, mechanical properties and osteoconductive properties and lower degradation rates. Different methods have been carried out for the preparation of nanocomposite materials such as chemical precipitation, sol-gel, hydrothermal, microemulsion and phase separation.

However, biomimetic processes are majorly used to form carbonated hydroxyapatite with desired characteristics of high surface area [10,11].

In this work, the several kinds of composite powders like HAP-PVA, HAP-PVP and HAP/PVA-PVP were prepared using PVA, PVP and hydroxyapatite. The biodegradability and mechanical strength of these composite powders have been compared with the respective individual polymers. The synthesized nanocomposites were characterized by FT-IR, XRD and thermal analysis (TGA/DSC). Nanosized HAP particles were observed by SEM analysis and the elemental composition of hydroxyapatite with various polymers was evidenced by EDAX analysis. Additionally, *in vitro* cytocompatibility assessment was carried out by using MG-63 Osteoblast cells for 24 and 48 h to prove the use of composite materials for better biomedical applications.

EXPERIMENTAL

Materials used for this study were polyvinyl alcohol (PVA) and polyvinyl pyrrolidone (PVP), calcium nitrate tetrahydrate ($Ca(NO_3)_2{\cdot}4H_2O$), ammonium dihydrogen orthophosphate, ammonia, ethanol and the chemicals to prepare simulated body fluid (SBF) solution were obtained from SDFCL, Mumbai, India.

Synthesis of nanocomposite: Nano-hydroxyapatite was prepared by co-precipitation technique and was blended with PVA and PVP as reported by Oudadesse *et al.* [12,13]. Initially, the composites were synthesized by mixing PVA and PVP in double distilled water followed by calcium nitrate tetrahydrate was progressively added to the polymer solution beneath assiduous aggregate and stirring for about 3 h at 90 ºC. To this solution, ammonium dihydrogen orthophosphate was added slowly under stirring condition and the pH of the solution was adjusted to 10 by adding ammonia. A dull white precipitate was formed after the addition of phosphorous precursor and the resultant suspension was left on stirring for 24 h. After decantation, the precipitate obtained was centrifuged at 4500 rpm and washed with double distilled water and then dried overnight in an oven at 60 ºC.

Simulated body fluid (SBF) immersion: For the *in vitro* bioactivity tests, 30 mg of powder was dissolved in 60 mL of simulated body fluid (SBF) prepared with Kokubo's protocol [14], which has mineral composition in close approximation to that of human plasma (Table-1).

TABLE-1
SBF SOLUTION PREPARATION (1 L)

Chemicals	Quantity
Ultrapure water	1 L
NaCl	7.996 g
$NaHCO_3$	0.350 g
KCl	0.224 g
$K_2HPO_4{\cdot}3H_2O$	0.228 g
$MgCl_2{\cdot}6H_2O$	0.305 g
$CaCl_2$	0.278 g
Na_2SO_4	0.071 g
$(CH_2OH)_3(NH_2){\cdot}HCl$	6.057 g

The prepared composite was immersed in SBF solutions and kept in an incubator at 37 ºC along with shaking at 50 rpm. The solution was refreshed with fresh SBF solution every 24 h. Finally, the precipitates were filtered (at different duration of immersion state such as 4, 7 and 15 days) and washed with deionized water to stop the apatite formation and washed with ethanol for completing the reaction. Samples were kept in an oven at 60 ºC until it was dried overnight. The Ca/P ratio was calculated by the following equations [15]:

$$\text{Mole fraction of Ca} = \frac{\text{Weight percent of Ca}}{\text{Molecular weight of Ca}} \quad (1)$$

$$\text{Mole fraction of P} = \frac{\text{Weight percent of P}}{\text{Molecular weight of P}} \quad (2)$$

$$\text{Final molar ratio of Ca/P} = \frac{\text{Mole fraction of Ca}}{\text{Mole fraction of P}} \quad (3)$$

Hemolytic assay: In this assay, 5 mL of blood was collected from the healthy volunteer, before receiving blood it has been informed to the consent person to participate in this study. And this study was perfomred on the principles of the Declaration of Helsinki as per the institutional ethical clearance (Ref. No: IVIT/CB-002/01/2022). After collecting, the blood sample has to be immediately transferred to 0.3% of EDTA solution to avoid coagulation. The blood sample was centrifuged at 10,000 rpm for 5 min to separate the RBCs from the solution. The RBCs (obtained pellet) were washed using phosphate buffer solution (PBS). This isotonic buffer washing procedure was followed continuously for three times. Polymer composite (1 mg) was weighed and dispersed in 1 mL of distilled water followed by the addition of 200 µL of prepared hemolytic sample and then transferred to a centrifuge tube. The positive control was prepared by mixing 200 µL RBC solution and distilled water, while the negative control was prepared by mixing 200 µL RBC and PBS solutions. These samples were kept at room temperature for 30 min and then were centrifuged at 10,000 rpm for 10 min. Finally, the optical density (OD) of the supernatant solution was measured at 540 nm. The hemolysis content (%) was obtained *via* following equation [16]:

$$HR = \frac{(D_t - D_{nc})}{(D_{pc} - D_{nc})} \times 100 \quad (4)$$

where D_t = sample absorbance, D_{nc} = negative control and D_{pc} = positive control.

MTT assay: The synthesized nanopowder were used for the cell viability and cell proliferation study using osteosarcoma (MG-63) cells by MTT assay. The sterilized composite powder samples (100 mg/mL) and 1×10^4 of MG-63 were filled in the 96 well culture plate and incubated at 37 ºC under CO_2 for 24 and 48 h. The culture plate was placed in the laminar flow chamber after incubation of 24 and 48 h. Further, the minimum Eagle's medium takes off from the culture plate using Pasteur pipette. The mixture of MTT agent and culture medium with a volume ratio of 1:39 was added into the each well of the culture plate. The MTT and culture medium was removed from each well after the incubation of dark condition for 4 h at room temperature. A 0.1 M of 70 µL PBS solution was filled in each well and absorbance of recorded at 570 nm using ELISA reader.

FT-IR analysis: FT-IR analysis was used to distinguish species and analyze the functional groups, vibration modes, chemical interaction of HAP with polymers. Evaluation by using FT-IR was accomplished using SHIMADZU CROP IRAFFINITY-1 Fourier transform infrared spectrophotometer within the variety 4000-400 cm^{-1}.

XRD analysis: The X-ray diffraction was used to identify the nanoparticles in composites. This characterization was performed for dried and finely tailored nano composite samples on XRD machine (BRUKER Germany with Cu*K*α radiation; λ = 1.5405 Å).

Thermal analysis: Thermal stability of the samples were studied by analyzing thermogravimetric curves obtained from a TGA equipment model SDT Q600 V20.9 Build 20, which uses pattern weight of 3-4 mg, RT > 1200 ºC @ 20 ºC/min N_2 Purge =100 mL. The initial, final and maximum degradation temperatures were defined.

DSC was carried out in a Shimadzu DSC-50 system with underneath flowing nitrogen (100mL/min) atmosphere at 20 k/min. All the analytical measures were carried out in replica. The melting enthalpy of HAP-PVA, HAP-PVP and HAP/PVA-PVP samples were computed from the peak field of the melting peak in the DSC curves, which was used to study the crystalline structure and glass transition temperature.

SEM-EDS analysis: ZISS-EVO18 scanning electron microscope was used to investigate the morphology of composite powders at excessive magnification and resolution by using lively electron beam.

RESULTS AND DISCUSSION

FTIR studies: Fig. 1a-d shows the FTIR spectra accomplished for the samples (HAP, HAP-PVA, HAP-PVP and HAP/PVA-PVP), respectively. The presence of $CaCO_3$ and HAP was confirmed due to the presence of bands at 561 cm^{-1} and 604 cm^{-1} and are the consequence of the ν_4 vibration associated with O-P-O modes in pure HAP (Fig. 1a). A weak peak at 696 cm^{-1} account to –OH bands, which demonstrate the existence of water in the composites. A strong band observed at 1025 cm^{-1} and weak band observed at 1251 cm^{-1} corresponds to the PO_4^{3-} functional group in HAP structure. Smaller peaks observed at 1355 cm^{-1} and 1731 cm^{-1} corresponds to the CO_3^{2-} functional group. The existence of carbonate particles identified in sample, would be a result of environmental carbon dioxide interacted with HAP antecedents in the blend mixture. The peaks observed at 3011 cm^{-1} and 3419 cm^{-1} were due to the presence of water, which might be due to vibration of OH^- ions in the HAP crystal grid. In HAP-PVA composite, a small peak at 3593 cm^{-1} indicates the presence of OH group (hydroxyl group) (Fig. 1b). The peak at 2792 cm^{-1} confirmed CH_2 asymmetric stretching and the peak at 1055 cm^{-1} indicates the presence of phosphate moiety in HAP structure [17]. Further, the peak at 1689 cm^{-1} confirmed the existence of C=O stretching bond in polyvinyl group.

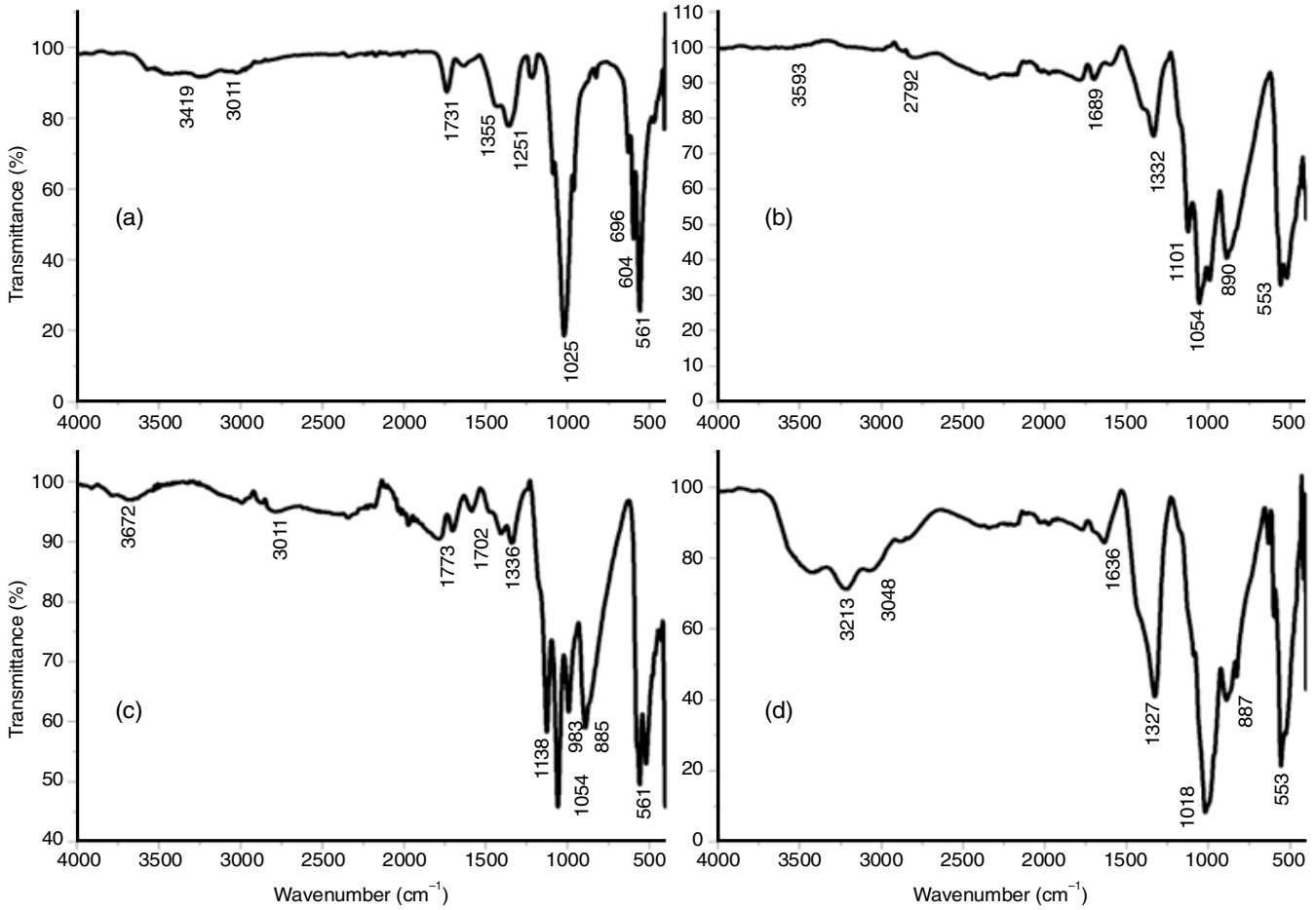

Fig. 1. FT-IR spectra of (a) HAP, (b) HAP-PVA, (c) HAP-PVP and (d) HAP-PVA-PVP

Similarly, in HAP-PVP composite, the OH stretching peak was observed at 3672 cm^{-1} (small peak) and 1773 and 1702 cm^{-1} peaks indicate the presence of C=O stretching in the polymeric network. The peak at 2904 cm^{-1} indicates C-H asymmetric stretching, CH_2 bending vibrations peak was observed at 1336 cm^{-1}. Additionally, the peak at 1138 cm^{-1} indicates the existence of C-N vibration in PVP structure (Fig. 1c). In the spectrum of HAP-PVA-PVP (Fig. 1d). A peak at 1636 cm^{-1} confirms the presence of C=O stretching in polyvinyl group, while a peak at 983 cm^{-1} confirms the presence of C-H asymmetric stretching in PVP in the polymer composite made with HAP-PVA-PVP.

XRD studies: Fig. 2 shows the XRD patterns of the prepared HAP, HAP-PVA, HAP-PVP and HAP-PVA-PVP nanocomposites. All the characteristics peaks of HAP are observed in the XRD spectrum. The major triplet peak at 2θ = 31.91º (211), 32.01º (112), 32.11º (300) are found to be well pronounced in all the composite with various polymeric network [18]. All the HAP peaks are found to be exist irrespective of the polymeric network. The intensity of HAP peak was confirmed in each of the composite HAP-PVA, HAP-PVP and HAP-PVA-PVP samples, respectively.

The presence of all fundamental HAP peaks at 25.99º (002), 28.19º (102), 28.99º (210), 31.98º (211), 32.05º (112), 32.19º (300), 39.81º (310), 42.11º (311), 43.9º (113), 45.87º, 46.32º (222), 48.90º (312) and 55.06º (321) in all the samples peak is in close approximation to the standard XRD pattern of HAP (ICDD: 89-6440). The peaks around 2θ = 17.5º were found to be polymer composite from samples HAP-PVA, HAP-PVP and HAP-PVA-PVP.

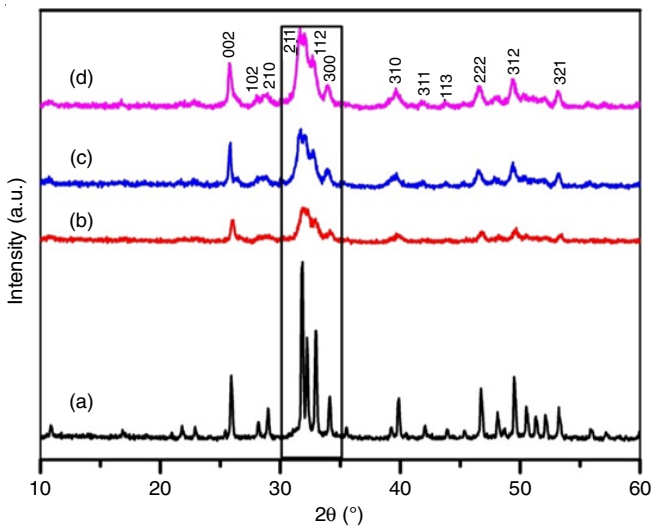

Fig. 2. XRD bands of (a) HAP, (b) HAP-PVA, (c) HAP-PVP and (d) HAP-PVA-PVP

Thermal studies: All the powder samples were subjected to TGA-DSC analysis to predict the thermal stability in Fig. 3. The weight loss percentage was found to be increased in the following order: 10% for (HAP), 25% for (HAP-PVA), 28% for (HAP-PVP) and 40% for (HAP-PVA-PVP), respectively. The polymer composite has a degradable property which was confirmed with weight loss of the prepared samples. The initial stage weight loss was observed from 100 to 200 ºC for all the respective samples. This weight loss might be due to the removal of moisture content in the powder sample. The second stage

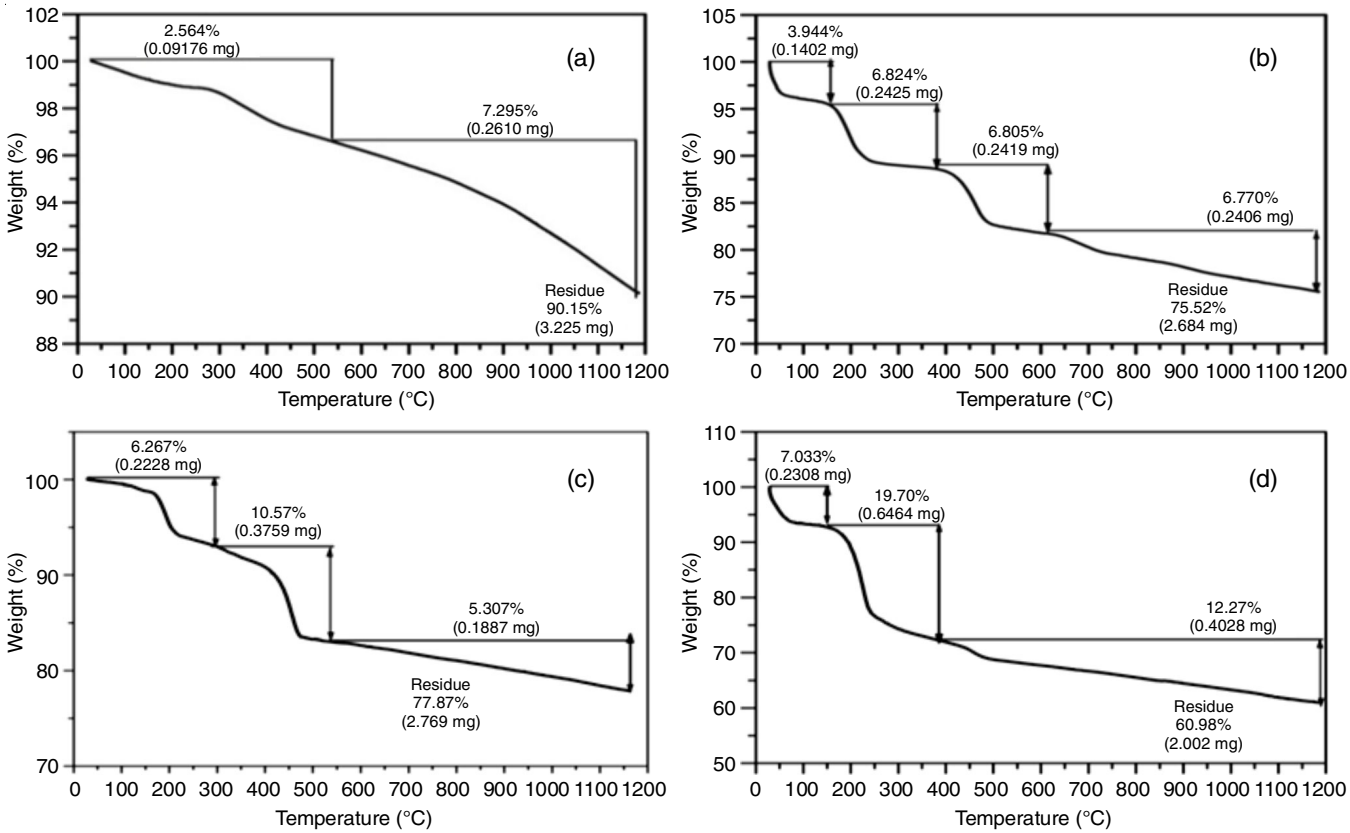

Fig. 3. TGA curves of (a) HAP, (b) HAP-PVA, (c) HAP-PVP and (d) HAP-PVA-PVP

of weight loss is due to the fundamental decomposition range at 200 to 300 ºC which might be due to the removal of polymer side chain and remaining observed water (OH).

Accurately, the weight loss of HAP was found at 290 ºC, whereas for in polymer composites, the decomposition stage was shifted to 300 ºC for HAP-PVA, 379 °C for HAP-PVP and 380 ºC for HAP-PVA-PVP composites. This might be due to the degradation of polymeric network from the powder samples. Third stage of decomposition had occurred at 400-600 ºC. This decomposition might be due to the degradation of polymer main chain. The HAP-PVA sample was found to decomposed at 478 ºC, HAP-PVP was decomposed at 540 ºC and HAP-PVA-PVP decomposed at 450 ºC [10]. For pure HAP, there is no evident decomposition occurred after 400 ºC, whereas the removal of the polymeric network from the sample indicates the different stages of decomposition. The samples with PVA have an additional decomposition at 600 ºC, which may be due to weak network of the polymer PVA (Table-2). Finally, the thermogravimetric results reveals HAP with polymer composite degrades at higher temperature compared to pure HAP [19,20].

TABLE-2
TGA WEIGHT LOSS PERCENTAGES CALCULATED FOR (1) HAP (2) HAP-PVA (3) HAP-PVP (4) HAP-PVA-PVP

Sample	Weight loss (°C)				Weight loss (%)
	1st stage	2nd stage	3rd stage	4th stage	
HAP	120	290	–	–	10
HAP-PVA	150	300	478	600	25
HAP-PVP	180	379	540	–	28
HAP-PVA-PVP	190	380	450	–	40

In order to investigate the thermal stability of the synthesized HAP based composite with different polymers, DSC (Fig. 4) was carried out and the parameters such as glass transition temperature (T_g), melting temperature (T_m) and decomposition ranges were found to be increased when compared to the individual polymers (Table-3). This might be due to the addition of polymers, where HAP acts as a center or nuclei for the crystallization of polymer in each composite. When compared to individual polymers, the HAP-polymeric composite shows higher T_g, T_m and decomposition temperature,which might be due to the presence of crystalline HAP in the polymeric composite [21]. This result confirmed that the HAP-polymer composite serves as a potential candidate in tissue engineering applications.

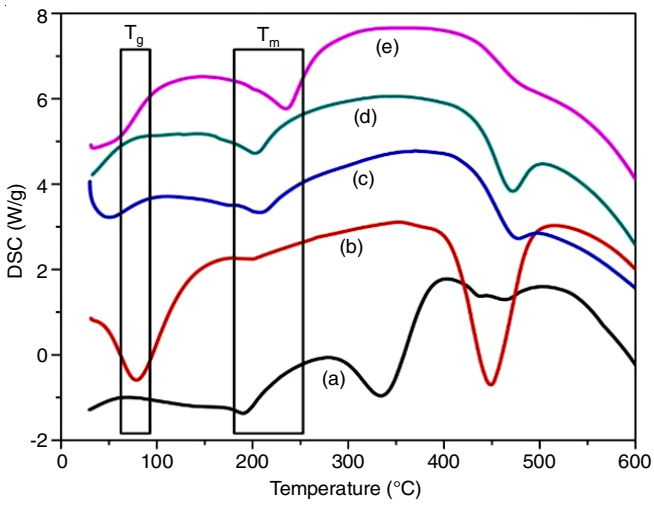

Fig. 4. DSC curves of (a) PVA, (b) PVP, (c) HAP-PVA, (d) HAP-PVP and (e) HAP-PVA-PVP

TABLE-3
PHYSICAL PROPERTIES FOR (1) PVA (2) PVP (3) HAP-PVA (4) HAP-PVP AND (5) HAP-PVA-PVP

Sample	Glass transition temperature (T_g) (°C)	Melting temperature (T_m) (°C)	Decomposition stage (°C)
PVA	61	190	437
PVP	153	201	447
HAP-PVA	71	205	472
HAP-PVP	96	220	474
HAP-PVA- PVP	105	234	484

Morphology studies: The SEM with EDAX images of HAP, HAP-PVA, HAP-PVP and HAP-PVA-PVP before and after immersion in SBF are shown in Fig. 5. Before and after SBF immersion, HAP represents uniform particle shape (Fig. 5a). Fig. 5b represents the sample with PVA. After immersion into SBF, the apatite layer was found to form on the surface in the form of spherical structure. Fig. 5c represents the presence of sample with PVP as a polymer. After SBF immersion, the rod like particles are found to be completely covered the surface. Fig. 5d represents the combination of PVA-PVP in

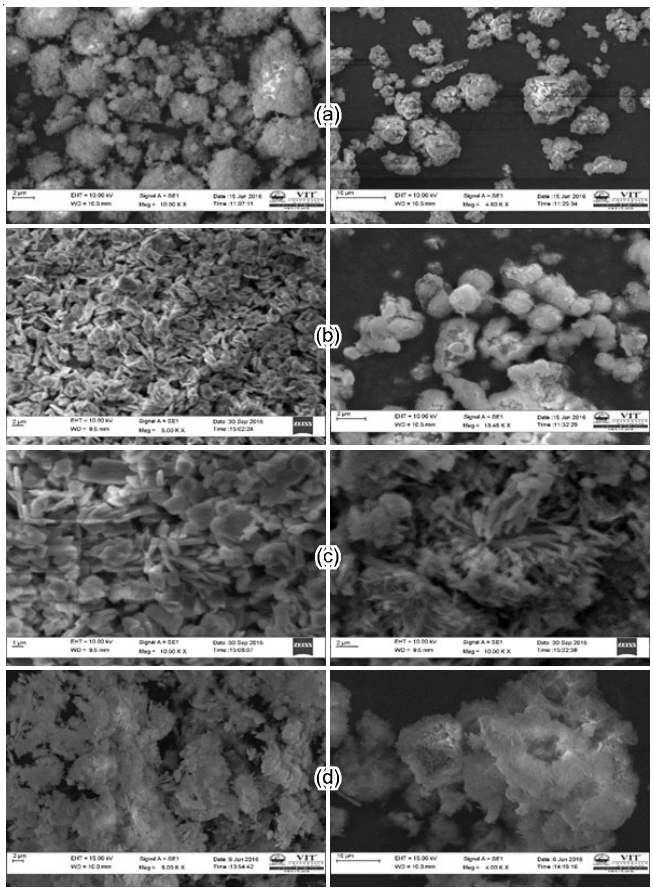

Fig. 5. SEM analysis of before and after immersion (a) HAP, (b) HAP-PVA, (c) HAP-PVP and (d) HAP-PVA-PVP

the HAP matrix. As observed from the SEM morphology, the presence of PVP polymer in the sample leads to the formation of rod like structure during SBF immersion. Further, the dissolution of polymeric network may be considered as important parameter may favour the cell adhesion and proliferation on the surface. Hence, the combination of HAP with PVP polymer indicates major changes in the apatite formation during *in vitro* bioactivity test.

The elemental compositions of the powder samples were evaluated through EDAX spectra (Fig. 6). The spectra were recorded before and after immersion in SBF solutions. The outcome of Ca/P ratio obtained after SBF immersion was influenced by the presence of polymeric network. Before immersion, the Ca/P ratio was found to be around 1.67 for pure HAP and found to increase to 1.68 after immersion in SBF solution. Irrespective of the polymeric network, the Ca/P ratio was found to be increased; this may be due to the formation of apatite layer over the surface. Hence, it is inferred that the polymer may provide site for the ionic interaction between the solution and the powder sample. The increase in Ca/P ratio of more than 1.72 reveals the formation of hydroxyl carbonated apatite on the surface.

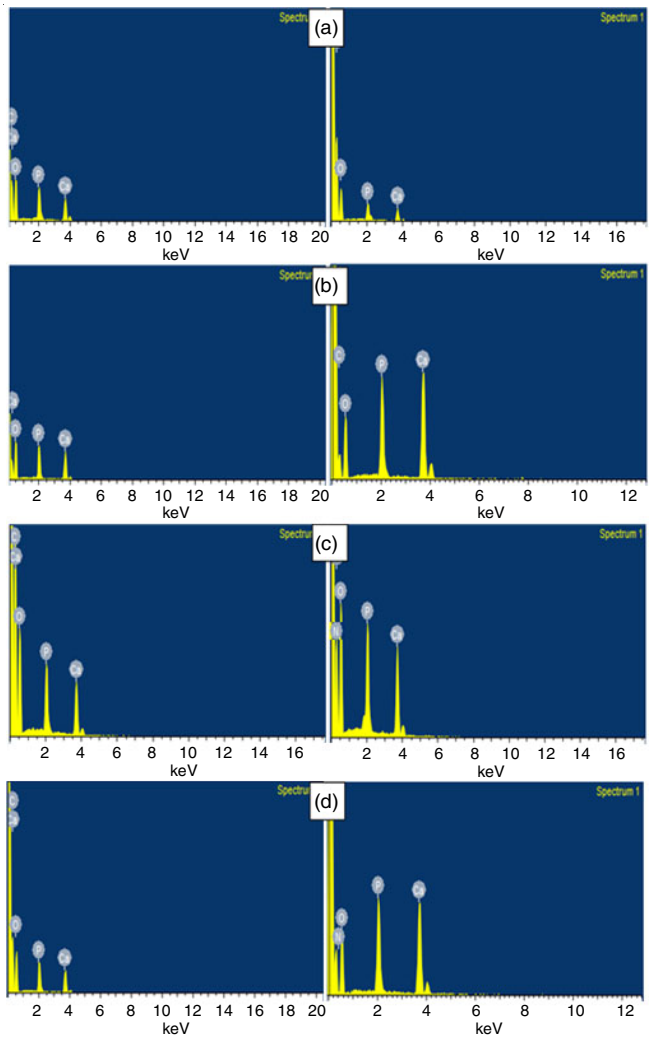

Fig. 6. EDAX analysis of before and after immersion (a) HAP, (b) HAP-PVA, (c) HAP-PVP and (d) HAP-PVA-PVP

XRD studies (after immersion): In order to confirm the phase formation, the XRD analysis (Fig. 7) was carried out for the SBF immersion samples. After immersion in SBF solution, the triplet peaks of HAP at 31.90º (211), 32.01º (112) and 32.17º (300) was found to be well-developed, which confirms the formation of carbonated HAP layer on the surface of composite [22]. With respect to the immersion period (4, 7 and 15 days), the intensity of HAP peaks was found to be well pronounced.

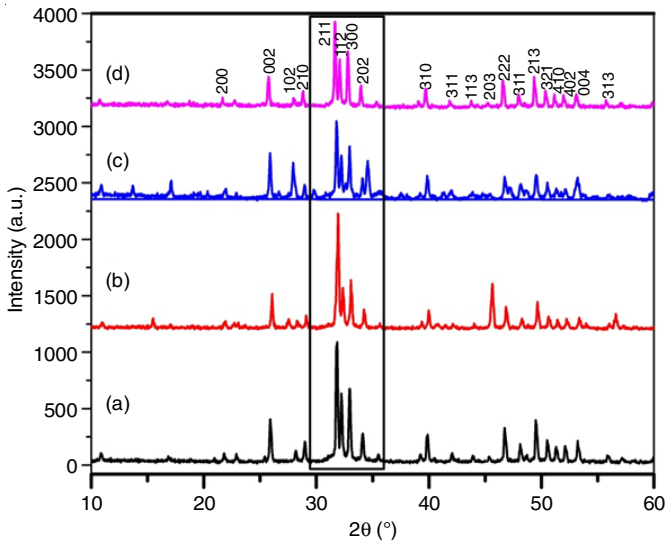

Fig. 7. XRD analysis of after immersion (a) HAP, (b) 7days, (c) 15 days and (d) 30 days of HAP-PVA-PVP

Finally, the XRD pattern indicates the growth of an apatite layer on the surface due to the nucleation process between the solution and the polymeric composite. The above results indicate the amorphous nature after immersion in SBF solution and for all the polymeric composites, the HAP structure was found to retain without any other secondary phases. Therefore, these polymeric composites can be found to be an appropriate material for bone regeneration, as the polymer plays a significant role in the formation of the apatite layer by dissolution.

In vitro study

Hemolytic assay: *In vitro* hemocompatibilty study, the individual components of HAP, HAP-PVA, HAP-PVP and HAP-PVA-PVP samples were examined with human blood, which can cause damage to the membrane of blood cells and release of hemoglobin. The result obtained from the test was summarized in Table-4. If the hemolysis proportion was less than 10%, the sample is considered to be slightly hemocompatible or less toxic, if the ratio is less than 5%, then considered

TABLE-4
HEMOLYTIC RATE (%) OF COMPOSITES

Sample	Absorbance	Hemolysis (%)
Negative control	0.25	–
Positive control	1.25	–
HAP	0.27	2
HAP-PVA	0.28	3
HAP-PVP	0.30	4
HAP-PVA- PVP	0.27	3

as hemocompatible or if less than 2%, then considered as highly hemocompatible or non-toxic [23].

From Table-4, it was inferred that the hemolytic rate less than 2% was obtained for HAP and hence it is confirmed to be highly hemocompatible or non-toxic. Moreover, the hemolytic rate was found to increases slightly with the addition of polymers. The HAP-PVA sample have shown a hemolytic ratio of 3% and the presence of PVP in HAP matrix have gave the ratio as 4%. Hence, the presence of polymer does not alter the hemocompatibilty of HAP. Finally, the combination of PVA-PVP has shown highly hemocompatible with the ratio of 3%. Further in order to prove the biocompatibility of the synthesized polymeric composition, it was subjected to *in vitro* cell culture analysis is MG-63 osteoblast cell line.

Cell viability: Fig. 8 represents the biocompatibility evaluation of various polymeric composite on MG-63 osteoblast cell lines. The prepared samples were found to be less toxic at 24 h and more proliferation of cells was takes place at 48 h of study. According to the results, the HAP-PVA-PVP sample exhibits more proliferation at both 24 and 48 h than HAP-PVA and HAP-PVP samples. The cell spreading on the surface was more elongated and spindle shaped morphology with cell to cell contact was observed from the microscopic evaluation, which may be due to the degradation of polymers in the composite, by making ways for the cell to proliferate at faster rate. These results clearly proved that the combination of HAP-PVA-PVP sample shows better cell attachment and proliferation, which was further observed by the phase contrast microscopy. Thus, this combination, may be suitable for bone regeneration application.

Conclusion

The biodegradability and hemocompatibility of the newly hydroxyapatite composites prepared with polyvinyl alcohol (PVA) and polyvinyl pyrrolidone (PVP) were investigated in this study. From the XRD results, it was observed that all the SBF immersed sample have led to hydroxyl carbonated apatite layer by dissolution of polymeric network. The triplet peak at 2θ = 31.91 (211), 32.01 (112), 32.11 (202) are found to be well pronounced as the immersion period increased to 15 days with amorphous nature. The T_g, T_m and decomposition stages of all the composite were compared by thermal analysis. With respect to the incorporation of polymer in the HAP matrix, the decomposition temperature was found to be increased. From SBF immersion, it was observed that the presence of PVP in the sample leads to the formation of rod like structure and the surface was found to be completely covered by HCA particles. The hemolytic ratio of 3% was observed for the HAP-PVA-PVP polymer denotes the compatibility in human blood. Hence, the biocompatibility of HAP-PVA-PVP leads to more proliferation of osteoblast cell for different duration of time. The longer duration at 48 h leads to the more cell proliferation and differentiation, this may favour the sample for tissue engineering applications.

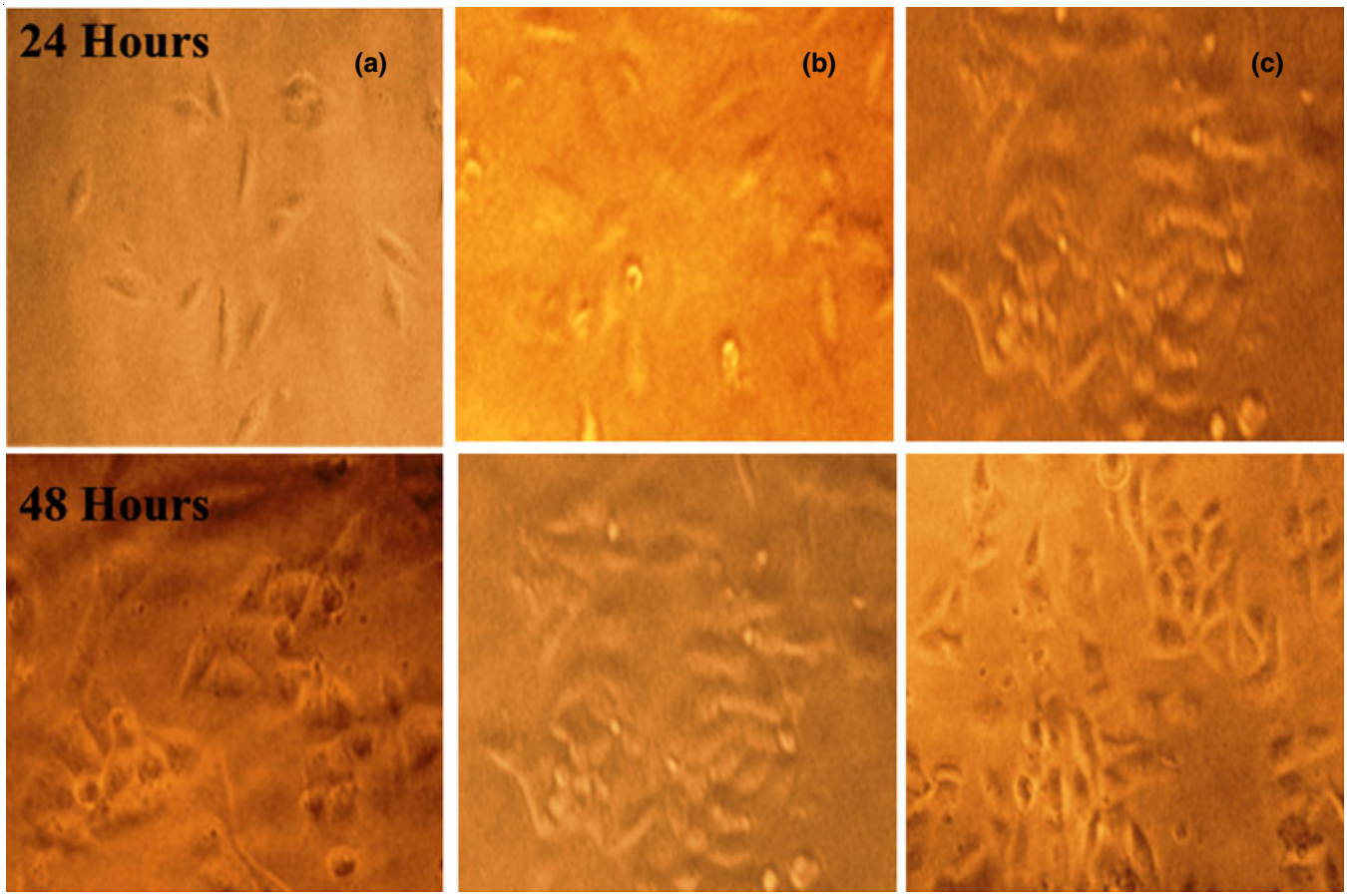

Fig. 8. Cell viability of (a), HAP-PVA, (b) HAP-PVP and (c) HAP-PVA-PVP

ACKNOWLEDGEMENTS

The authors thank the Management of VIT University, Vellore, India for rendering the necessary research facilities. One of the authors highly acknowledges the DST (File No. EMR/2016/002562) for the financial support.

CONFLICT OF INTEREST

The authors declare that there is no conflict of interests regarding the publication of this article.

REFERENCES

1. R.Y. Basha, S.K. Sampath and M. Doble, *Mater. Sci. Eng. C*, **57**, 452 (2011); https://doi.org/10.1016/j.msec.2015.07.016
2. S.M. Stella, T.M. Sridhar, R. Ramprasath, J. Gimbun and U. Vijayalakshmi, *Polymers*, **15**, 155 (2022); https://doi.org/10.3390/polym15010155
3. B. Dhandayuthapani, Y. Yoshida, T. Maekawa and and D.S. Kumar, *Int. J. Polym. Sci.*, **2011**, 290602 (2011); https://doi.org/10.1155/2011/290602
4. S.U. Maheshwari, V.K. Samuel and N. Nagiah, *Ceram. Int.*, **40**, 8469 (2014); https://doi.org/10.1016/j.ceramint.2014.01.058
5. N. Ramesh, S.C. Moratti and G.J. Dias, *J. Biomed. Mater. Res. B Appl. Biomater.*, **106**, 2046 (2018); https://doi.org/10.1002/jbm.b.33950
6. S.M. Stella and U. Vijayalakshmi, *J. Biomed. Mater. Res. A*, **107**, 610 (2019); https://doi.org/10.1002/jbm.a.36577
7. A. Asti and L. Gioglio, *Int. J. Artif. Organs*, **37**, 187 (2014); https://doi.org/10.5301/ijao.5000307
8. J.M. Dodda, P. Bìlský, J. Chmelaø, T. Remiš, K. Smolná, M. Tomáš, L. Kullová and J. Kadlec, *J. Mater. Sci.*, **50**, 6477 (2015); https://doi.org/10.1007/s10853-015-9206-7
9. M.A.-F. Basha, *Polym. J.*, **42**, 728 (2010); https://doi.org/10.1038/pj.2010.60
10. C.A. Charitidis, A. Skarmoutsou, A. Tsetsekou, D. Brasinika and D. Tsiourvas, *Mater. Sci. Eng. B*, **178**, 391 (2013); https://doi.org/10.1016/j.mseb.2013.01.002
11. M. Navarro, A. Michiardi, O. Castaño and J.A. Planell, *J. R. Soc. Interface*, **5**, 1137 (2008); https://doi.org/10.1098/rsif.2008.0151
12. H. Oudadesse, Y.L. Gal, O. Merdrignac-Conanec, G. Cathelineau and X.V. Bui, *Korean J. Chem. Eng.*, **29**, 215 (2012); https://doi.org/10.1007/s11814-011-0151-0
13. A. Mostafa, H. Oudadesse, M.B. Mohamed, E.S. Foad, Y. Le Gal and G. Cathelineau, *Chem. Eng. J.*, **153**, 187 (2009); https://doi.org/10.1016/j.cej.2009.05.039
14. T. Kokubo, H. Kushitani, S. Sakka, T. Kitsugi and T. Yamamuro, *J. Biomed. Mater. Res.*, **24**, 721 (1990); https://doi.org/10.1002/jbm.820240607
15. C.H. Yeo, S.H.S. Zein, A.L. Ahmad and D.S. McPhail, *Braz. J. Chem. Eng.*, **29**, 147 (2012); https://doi.org/10.1590/S0104-66322012000100016
16. A.F. Leitão, S. Gupta, J.P. Silva, I. Reviakine and M. Gama, *Colloids Surf. B Biointerfaces*, **111**, 493 (2013); https://doi.org/10.1016/j.colsurfb.2013.06.031
17. N. Krishnamacharyulu, G. Jagan Mohini, G. Sahaya Baskaran, V. Ravi Kumar and N. Veeraiah, *J. Alloys Compd.*, **734**, 318 (2018); https://doi.org/10.1016/j.jallcom.2017.10.271
18. M. Rama and U. Vijayalakshmi, *J. Drug Deliv. Sci. Technol.*, **61**, 102182 (2021); https://doi.org/10.1016/j.jddst.2020.102182
19. C. Guo, L. Zhou and J. Lv, *Polym. Polymer Compos.*, **21**, 449 (2013); https://doi.org/10.1177/096739111302100706
20. J. Rodríguez, E. Navarrete, E.A. Dalchiele, L. Sánchez, J.R. Ramos-Barrado and F. Martín, *J. Power Sources*, **237**, 270 (2013); https://doi.org/10.1016/j.jpowsour.2013.03.043
21. M.B. El-Arnaouty, M. Eid, M. Salah and E.-S.A. Hegazy, *J. Macromol. Sci. Part A Pure Appl. Chem.*, **49**, 1041 (2012); https://doi.org/10.1080/10601325.2012.728466
22. B. Priyadarshini and U. Vijayalakshmi, *Mater. Sci. Eng. C*, **119**, 111620 (2021); https://doi.org/10.1016/j.msec.2020.111620
23. Chetan and U. Vijayalakshmi, *J. Biomed. Mater. Res. B Appl. Biomater.*, **108**, 3286 (2020); https://doi.org/10.1002/jbm.b.34665